Structure, Vol. 13, 29–41, January, 2005, ©2005 Elsevier Ltd All rights reserved. DOI 10.1016/j.str.2004.10.009

Siderocalin (Lcn 2) Also Binds Carboxymycobactins, Potentially Defending against Mycobacterial Infections through Iron Sequestration

Margaret A. Holmes,[1] Wendy Paulsene,[1] Xu Jide,[2] Colin Ratledge,[3] and Roland K. Strong[1,*]
[1]Division of Basic Sciences
Fred Hutchinson Cancer Research Center
Mail Stop A3-025
1100 Fairview Avenue North
Seattle, Washington 98109
[2]Chemistry Department
University of California, Berkeley
Berkeley, California 94720
[3]Department of Biological Sciences
University of Hull
Hull HU6 7RX
United Kingdom

Summary

Siderocalin, a member of the lipocalin family of binding proteins, is found in neutrophil granules, uterine secretions, and at markedly elevated levels in serum and synovium during bacterial infection; it is also secreted from epithelial cells in response to inflammation or tumorigenesis. Identification of high-affinity ligands, bacterial catecholate-type siderophores (such as enterochelin), suggested a possible function for siderocalin: an antibacterial agent, complementing the general antimicrobial innate immune system iron-depletion strategy, sequestering iron as ferric siderophore complexes. Supporting this hypothesis, siderocalin is a potent bacteriostatic agent in vitro under iron-limiting conditions and, when knocked out, renders mice remarkably susceptible to bacterial infection. Here we show that siderocalin also binds soluble siderophores of mycobacteria, including *M. tuberculosis*: carboxymycobactins. Siderocalin employs a degenerate recognition mechanism to cross react with these dissimilar types of siderophores, broadening the potential utility of this innate immune defense.

Introduction

Lipocalins are a functionally diverse group of binding proteins, widely expressed across multiple phyla, that share a conserved structure even in the absence of significant sequence conservation (Flower et al., 2000). This core structure consists of an eight-stranded antiparallel β barrel that defines a calyx, or cup-shaped structure, enclosing the ligand binding site, plus conserved α and 3_{10} helices (Flower, 1996). The loops linking the β strands are typically short β hairpins, except the first loop, which describes a large Ω loop that usually folds back onto the barrel, partially constricting the binding site. Lipocalins generally act as transporters (though some are enzymes), trafficking small molecules to specific cells and are thus proposed to be variously involved in retinol transport, invertebrate cryptic coloration, olfaction, pheromone transport, fatty acid transport, prostaglandin synthesis, modulation of cell growth and metabolism, regulation of the immune response, tissue development, and animal behavior (Åkerstrom et al., 2000a). Lipids or lipophilic molecules are common candidate ligands, hence the name "lipocalin," reflected in the apolar character of the lining of the calyx, generally a deep invagination into the protein core.

Siderocalin (Lipocalin 2) is deposited in late granules in neutrophil precursors and can be expressed highly in a variety of tissues, particularly epithelium (Kjeldsen et al., 2000). An acute phase protein in mice, siderocalin concentrations rise dramatically in serum (where its presence diagnostically differentiates between bacterial and viral infections [Xu and Venge, 2000]) and other bodily fluids in response to inflammatory signals or infection (Kjeldsen et al., 2000). Siderocalin has historically been variously referred to as neutrophil gelatinase associated lipocalin (NGAL), human neutrophil lipocalin (HNL), α_1-microglobulin related protein (human ortholog); 24p3, uterocalin, superinducible protein 24 (SIP24; murine ortholog); or *neu*-related lipocalin (NRL; rat ortholog) (Kjeldsen et al., 2000). Unlike the stereotypical lipocalin, structure determinations show that siderocalin has a broad, shallow calyx lined with polar and positively charged residues (Coles et al., 1999; Goetz et al., 2000, 2002). Siderocalin has been shown to specifically bind, with a subnanomolar dissociation constant (Goetz et al., 2002), the phenolate/catecholate-type enterobacterial ferric siderophore enterochelin (Raymond et al., 2003) (FeEnt, or Ent in its apo form, also referred to as enterobactin; Figure 1). Siderophores are low molecular weight (500–1000 Da), virtually ferric-specific chelators involved in microbial iron acquisition (Stintzi and Raymond, 2002; Winkelmann, 2002). Siderocalin is therefore proposed to function by complementing the general antibacterial iron-sequestration strategy of the innate immune system (Goetz et al., 2002). Siderocalin uniquely complements this strategy by binding iron already earmarked for bacterial use through its specificity for ferric siderophore complexes, rather than binding iron directly (Goetz et al., 2002), as does, for example, the bacteriostatic protein lactoferrin. Consistent with this proposal, siderocalin is a potent bacteriostatic agent in vitro under iron-limiting culture conditions (Goetz et al., 2002); siderocalin knock-out mice, in the absence of any other gross morphological, behavioral, or physiological defects, are also profoundly susceptible to bacterial infections with clinical isolates of *E. coli* (Flo et al., 2004). Both effects are due to the limitation of bacterial growth through iron depletion. Several studies have demonstrated the importance of such tissue- and pathogen-specific antimicrobial proteins in other systems. Human defensins and mouse cryptdins, secreted by Paneth cells in small intestinal crypts, provide protection against enteropathogenic *Salmonella* (Salzman et al., 2003; Wilson et al., 1999); mice deficient in the cathelicidin CRAMP, produced by neutrophils and skin keratinocytes, are more susceptible to cutaneous infections of group A strepto-

*Correspondence: rstrong@fhcrc.org

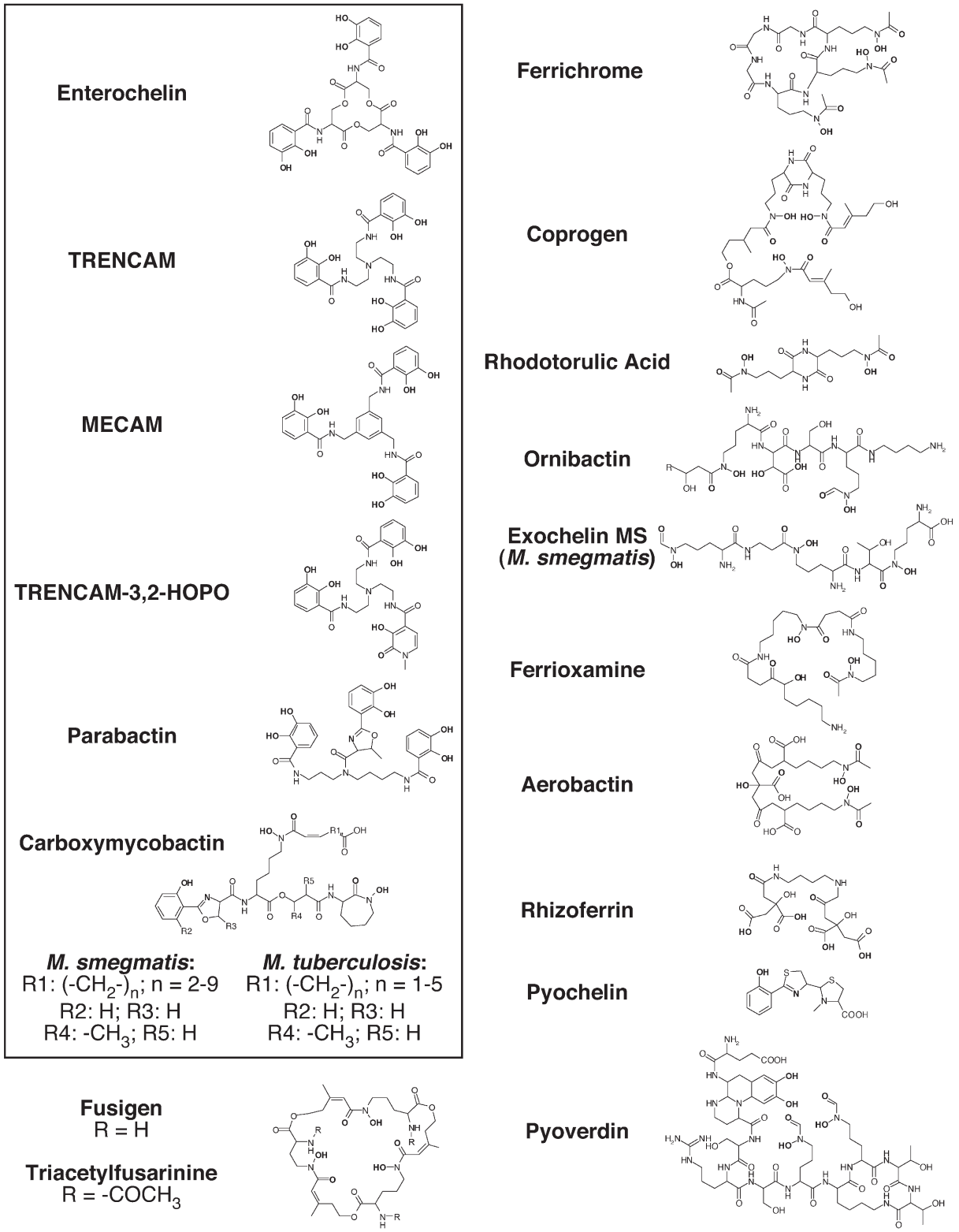

Figure 1. Siderocalin Binding Preference for Representative Siderophores

Compounds demonstrating tight binding in qualitative SPR-based (reported here or in Flo et al., 2004) or quantitative fluorescence quenching (Goetz et al., 2002) assays are boxed. Compounds are grouped by similar iron liganding chemistry: solely DHBA-based phenolate/catecholates (Ent through MECAM), mixed phenolates (TRENCAM-3,2-HOPO and parabactin), mixed phenolate/hydroxamates (CMBs), hydroxamates (fusigen through ferrioxamine), mixed hydroxamate/α-hydroxycarboxylic acid (aerobactin), α-hydroxycarboxylic acids (rhizoferrin), and the complex siderophores of *Pseudomonas*: pyochelin and pyoverdin. Iron ligands are shown in bold.

cocci (Nizet et al., 2001). However, the molecular mechanisms of these latter defenses remain to be fully elucidated.

While human siderocalin also associates, through a specific disulfide linkage, with matrix metalloproteinase-9 (MMP-9; also gelatinase B) in neutrophil granules (Kjeldsen et al., 2000), the only demonstrated consequence is a slight acceleration of the direct activation of promatrix metalloproteinases through a nonphysiological pathway (Tschesche et al., 2001). There is no noncovalent component to siderocalin/MMP-9 association (M.A.H., unpublished data), suggesting that the interaction may be serendipitous (murine siderocalin lacks the corresponding cysteine and is not known to associate with MMP-9). Murine siderocalin has also been implicated in processes as diverse as apoptosis (Devireddy et al., 2001), though the effect has only been demonstrated in a limited context (Kamezaki et al., 2003), and kidney cell differentiation (Yang et al., 2002), functioning through a transferrin-independent iron transport pathway by binding an endogenous, currently uncharacterized, mammalian "siderophore." Human-mouse-rat siderocalin pair-wise sequence identities are 60%–81%, where the pattern of conservation strongly implies conservation of ligand specificity (Goetz et al., 2002); no other obvious orthologs have been identified so far.

Here we show that unusual aspects of the siderocalin/siderophore recognition mechanism, dominated by hybrid electrostatic/cation-π interactions, permit degenerate recognition of (1) a range of catecholate siderophores chemically similar to Ent and (2) the soluble siderophores of mycobacteria, carboxymycobactins (CMBs), which are chemically distinct from Ent. (CMBs were originally referred to as "exochelins," though that term is now reserved for distinct, soluble siderophores of saprophytic mycobacteria [Figure 1].) The consequence of these results is broadening potential siderocalin-mediated antibacterial innate immune responses to include a wide array of pathogens. Defining the specificity of siderophore binding innate immune system components has additional implications for the association of certain siderophores with virulence and for proposals to use siderophores and siderophore analogs as therapeutics (Budzikiewicz, 2001; Horwitz et al., 1998; Roosenberg et al., 2000).

Results

Previous crystallographic studies of siderocalin showed that the protein recognizes FeEnt through a novel hybrid of ionic (Ent is uncharged, but FeEnt carries a net –3 charge [Raymond et al., 1984] delocalized over the molecule [Goetz et al., 2002]) and cation-π interactions, where the interacting groups are interlaced, alternating between cationic moieties and catecholates, in a cyclically permuted manner around the iron atom (Goetz et al., 2002) (Figures 2A and 3A). Cation-π bonds in proteins are interactions between the positive charge of lysine or arginine side chains and the quadrupole moment associated with the delocalized π electrons of an aromatic functional group such as tryptophan, tyrosine, or phenylalanine (Dougherty, 1996). In siderocalin, the cationic groups are donated by the side chains of three positively charged residues, Arg81, Lys125, and Lys134. The K_D for the interaction was measured at 0.4 nM at 22°C by fluorescence quenching (Goetz et al., 2002). The nature of siderocalin/siderophore interactions, where the siderophore is centered in the siderocalin calyx making multiple, direct, polar interactions, together with the tight affinity, clearly demonstrate specificity and is almost certainly not serendipity.

However, the structural analysis revealed two unusual aspects of the complex: (1) the quality of the electron density corresponding to the siderophore in all three monomers of the asymmetric unit was very poor, diffuse, and choppy; and (2) the fit of the siderophore into the calyx exposed much of the ligand to solvent and failed to fill several obvious, underlying pockets. The quality of the ligand electron density was so poor that FeEnt was best modeled as multiple conformations of partial structures representing FeEnt hydrolysis products, dihydroxybenzoic acid (DHBA), and serine-dihydroxybenzoate (DHBS), though intact FeEnt was also refined separately (Goetz et al., 2002) (Figure 2A). There are several possible explanations for the poor quality of the ligand density in an otherwise well-refined structure: (1) degradation of FeEnt, through hydrolysis and/or oxidation in solution, during the course of crystallization (almost 7 months); (2) less-than-complete ligand occupancy; and (3) ligand mobility; or some combination of these factors. The failure of FeEnt to completely fill the calyx also raised the possibility that siderocalin may also bind other ligands. Siderophores come in a bewildering array of variants that can be divided into three broad classes depending on the chemistry of chelation: hydroxamates, phenolates/catecholates, or α-hydroxycarboxylates (Figure 1)—though examples of yet other iron binding moieties are known. Therefore, the possibility exists that siderocalin may bind siderophores other than phenolate/catecholates, which would potentially broaden the range of affected pathogens.

Siderocalin Binding Does Not Constrain Phenolate Siderophores to a Defined Orientation

In order to control for ligand degradation, new crystallization conditions were found that yielded diffraction-quality crystals within weeks rather than months and at a lower pH (see Experimental Procedures). This new crystal form is nearly isomorphous with the neutral pH siderocalin/FeEnt complex crystals, with three molecules (A, B, and C) in the asymmetric unit. Siderocalin was also cocrystallized with two synthetic siderophores: TRENCAM, an analog of Ent, and TRENCAM-3,2-HOPO, similar to the natural siderophore cepabactin which contains a 1,2-hydroxypyridinone (HOPO) iron binding moiety (Figure 1 and Table 1) (Thulasiraman et al., 1998). HOPO moieties also reduce the net negative charge by one relative to DHBA groups, demonstrating that conservation of an overall net charge of –3 is not a requirement for siderocalin binding. These synthetic compounds, with different backbone chemistries, are far more resistant to hydrolysis in solution than natural siderophores with labile triserine trilactone backbones (Ecker et al., 1988, 1986; Matzanke et al., 1986). Ex-

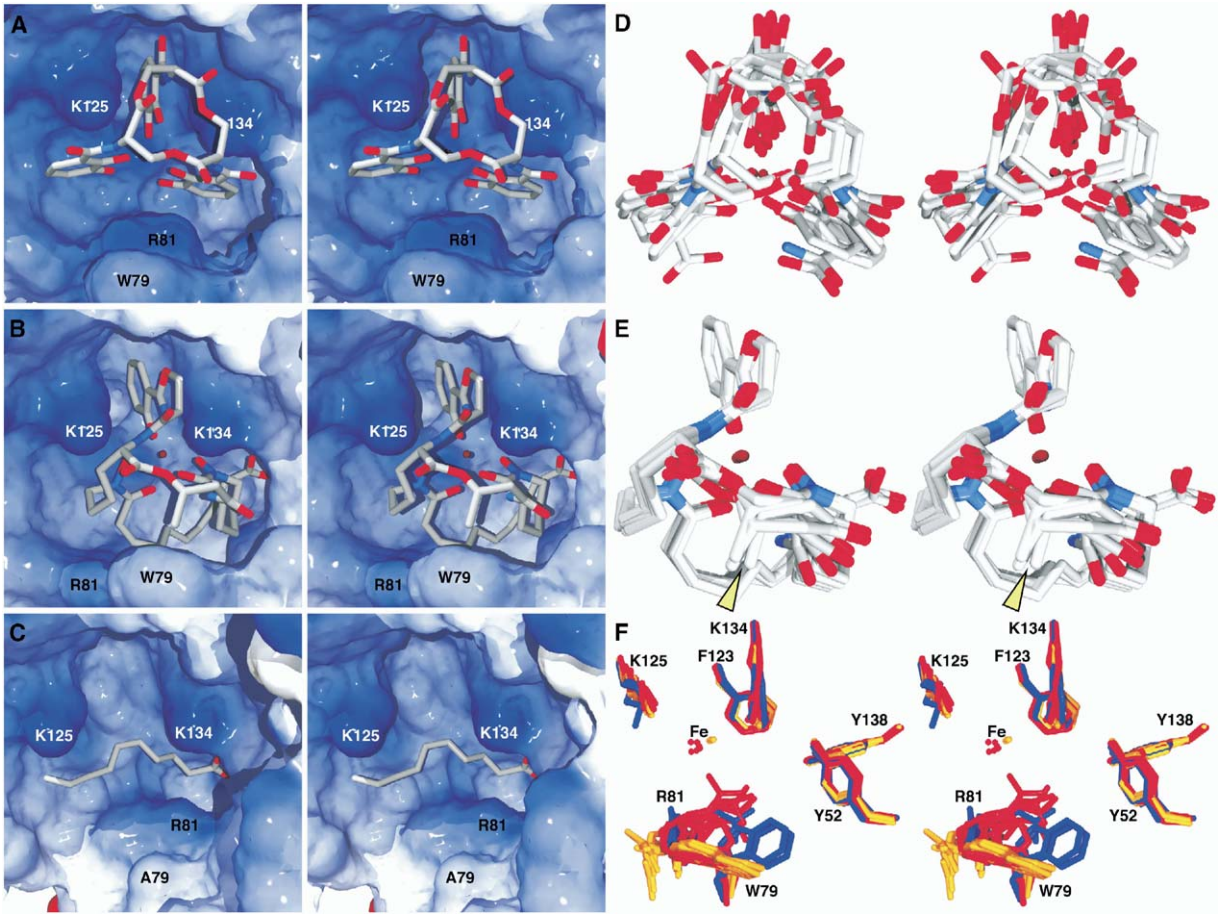

Figure 2. Stereoviews of Siderocalin Ligands Positioned in the Siderocalin Calyx

(A) Ent, (B), CMB-S, and (C), NCA. Ligands are shown in a licorice stick representation, colored by atom-type (C, gray; N, blue; O, red; Fe, dark red). The molecular surface of the protein (as displayed by SwissPDBViewer [Guex and Peitsch, 1997]) is shown, colored by electrostatic potential (positive, blue; negative, red). Surfaces corresponding to Trp79, Arg81, Lys125, and Lys134 are labeled. In these views, the three pockets of the trilobate siderocalin calyx are 1, at the top; 2, at the lower right; and 3, at the lower left. The deepest portion of the calyx is pocket 2.

(D and E) Stereoviews of superpositions (based only on protein atoms) of all of the different models of Ent and TRENCAM-3,2-HOPO (intact and partial structures) and the six total CMB-S/T models. The arrowhead indicates the position of the R4 methyl group, the only difference observed between the CMB-S and -T ligands in the complex crystal structures.

(F) Stereoview of the superposition of key ligand contacting side chains from the 15 available views of siderocalin from the crystal structures, colored by the ligand present in the complex (NCA or none, blue; phenolate-type siderophore, red; and CMBs, orange). The position of the iron atom varies by over 1.1 Å among the phenolate-type siderophore calyces and by no more than 0.46 Å among the CMB calyces. All molecular figures were generated with SwissPDBViewer (Guex and Peitsch, 1997) and rendered using the MegaPOV extensions (megapov.inetart.net) to POV-Ray (www.povray.org) except where noted.

aminations of the preliminary electron density maps, phased by molecular replacement (d_{min} = 2.5 or 2.1 Å, respectively), showed that the density corresponding to the ligands was as poor as in the initial FeEnt complex (data not shown). The conclusion is that while ligand degradation may contribute to poor ligand density, it does not solely account for the effect. The TRENCAM complex was therefore not refined, as the interaction with siderocalin appeared identical to FeEnt, though the TRENCAM-3,2-HOPO complex structure was fully refined (Table 1), as this compound represents a distinct siderophore type, again modeling the ligand using multiple substructures (dihydroxybenzamide). However, within the limitation of the poor quality of the density, TRENCAM-3,2-HOPO apparently also interacts with siderocalin identically to FeEnt (Figures 2A and 2D). (The quality of the density did not permit resolving the preferred position, if any, of the asymmetrical HOPO group of TRENCAM-3,2-HOPO in the siderocalin calyx.) The conservation of ligand orientation in the calyx confirms the observation that the "backbone" of the siderophore, which is completely different between the native and synthetic molecules, does not contribute significant protein contacts affecting binding (Goetz et al., 2002). This point is also supported by the high-affinity binding of MECAM, yet another synthetic Ent analog, with a third, distinct backbone structure (Figure 1).

Though the current complex crystallization condi-

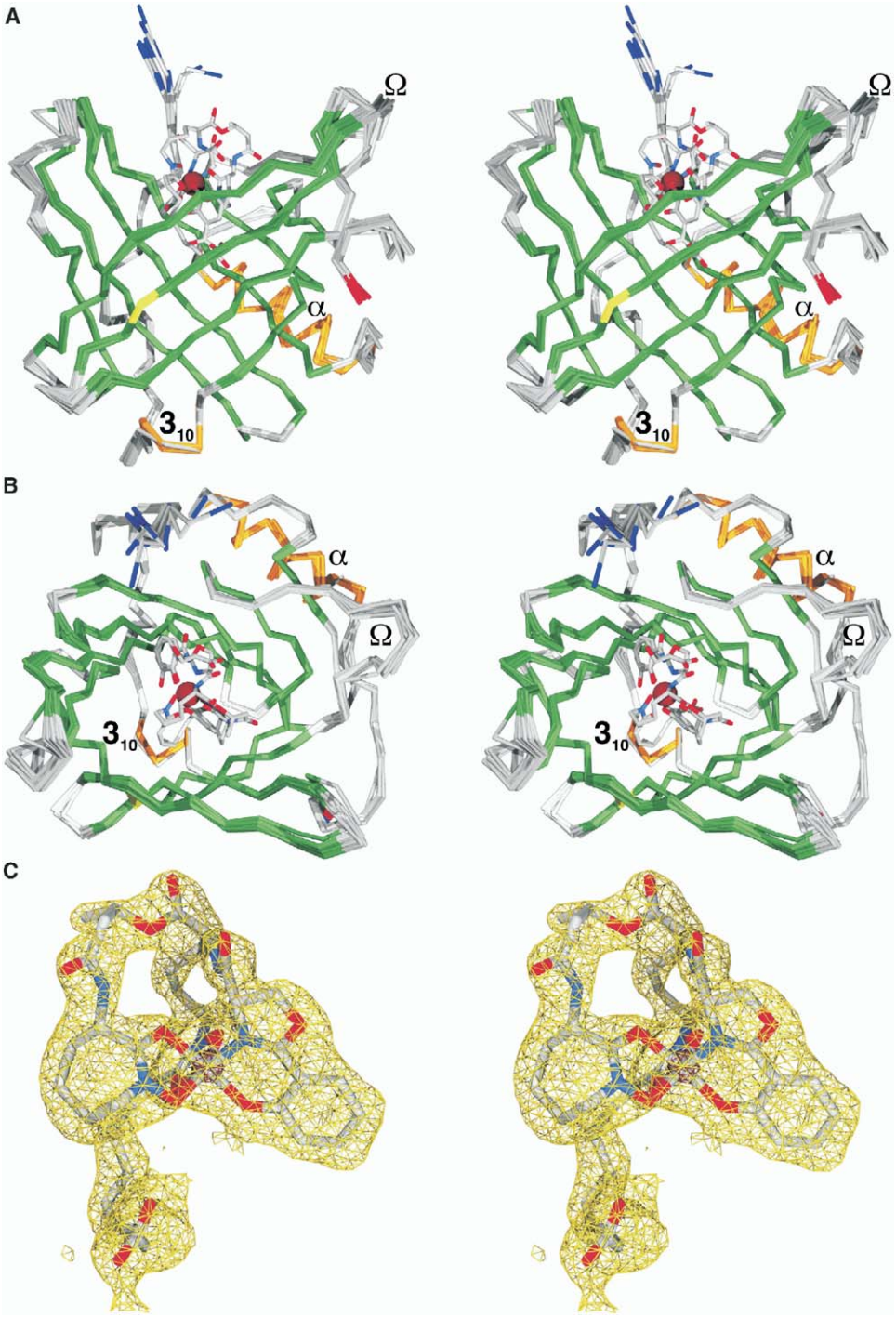

Figure 3. Binding of CMB-S to Siderocalin

(A and B) Stereoviews ([A], from the side; [B], from above, looking down into the calyx) of CMB-S bound to siderocalin. The protein is represented by a superposition of the Cα backbones of all fifteen independent views of siderocalin (from a total of six crystal structures, three reported here and three previously reported [Goetz et al., 2000, 2002]), colored by secondary structure (α, orange; β, green; and coil, gray). N termini are colored blue; C termini are colored red; the Cα of Asn65, the location of the single N-linked oligosaccharide, is colored yellow.

(C) Stereoview of the simulated annealing composite-omit $2F_{obs} - F_{calc}$ electron density map contoured around the CMB-S ligand (molecule C; C, gray; N, blue; and O, red) at 1σ (amber) and 8σ (dark red).

tions are at low pH (4.5), rather than neutrality, there is essentially no effect on the overall structure of the protein (Figures 3A and 3B). Catecholate-type siderophores are known to undergo a sequential shift in binding mode in solution, from phenolate-mode binding to salicylate-mode binding, concurrent with acidification,

Table 1. Crystallographic Statistics

Siderophore	TRENCAM-3,2-HOPO	TRENCAM	CMB-S	CMB-T
Data Collection				
Space group	$P4_12_12$	$P4_12_12$	$P4_12_12$	$P4_12_12$
Lattice constants (Å)	a = b = 114.4, c = 119.0	a = b = 115.1, c = 119.5	a = b = 114.2, c = 119.3	a = b = 114.8, c = 119.1
Resolution range (Å)	20.0–2.10 (2.14–2.10)[a]	20.0–2.50 (2.54–2.50)	20.0–2.10 (2.14–2.10)	20.0–2.20 (2.24–2.20)
Observations	456,603	204,054	381,305	418,554
Unique reflections	45,047	27,376	46,438	40,016
Completeness (%)	96.6 (93.0)	96.4 (98.4)	99.9 (100.0)	97.6 (99.4)
I/σ(I)	11.1 (1.5)	10.6 (2.8)	16.0 (2.9)	14.6 (2.6)
R_{sym} (%)	4.7 (39.9)	5.7 (41.3)	5.5 (34.5)	6.8 (37.5)
Fe peak heights[b] (A, B, C; σ)	9, 4, 6	11, 7, 14	11, 12, 17	17, 12, 18
Refinement Statistics				
R_{work} (%)	22.5	—	22.0	22.0
R_{free}[c] (%)	25.7	—	25.1	25.3
Number of atoms				
Protein	4,127	—	4,154	4,113
Siderophore	58	—	162	159
Waters	116	—	95	105
Estimated coordinate error[d] (Å)	0.24	—	0.20	0.23
Geometry				
Rmsd bonds (Å)	0.024	—	0.027	0.024
Rmsd angles (°)	2.2	—	2.2	2.2
Rmsd dihedrals (°)	27.5	—	27.3	27.2
Rmsd impropers (°)	1.4	—	1.6	1.4
Average B factor (Å^2)	38.3	—	38.3	37.1
Protein monomer B factors (A, B, C; Å^2)	33.3, 50.2, 28.8	—	33.9, 51.9, 27.2	31.9, 52.8, 26.1
Siderophore B factors (A, B, C; Å^2)	72.1, 85.6, 61.3	—	47.5, 59.2, 39.1	38.2, 59.0, 36.5
Water B factors (Å^2)	36.0	—	33.1	32.2
Ramachandran[e]				
Most favored (%)	90.2	—	90.7	90.5
Additional allowed (%)	8.4	—	7.9	8.0
Generously allowed (%)	0.0	—	0.0	0.5[f]
Disallowed (%)	1.3[f]	—	1.4[f]	1.1[f]

[a] Numbers in parentheses correspond to the highest resolution shell.
[b] Peak heights of electron density features associated with ligand iron atoms in simulated annealing composite-omit Fourier syntheses.
[c] Calculated on 10% of the data (Kleywegt and Brunger, 1996) and matched between data sets.
[d] Crossvalidated σ_A error as calculated in CNS (Brunger et al., 1998).
[e] Calculated with PROCHECK (Laskowski et al., 1992).
[f] The Ramachandran outliers are the same two residues (Y115 and C175) in all three molecules in all of the refined structures, despite careful rebuilding, arguing that these residues are not poorly modeled but truly adopt unfavorable conformations.

correlating with reduced iron affinity (Cohen and Raymond, 2000). The transition occurs one phenolate group at a time as pH decreases. FeEnt starts to shift at around a pH of 4.5. While poor, the electron density is good enough to argue that both TRENCAM and TRENCAM-3,2-HOPO remain in phenolate mode in the complex, suggesting that complexation with siderocalin stabilizes phenolate-mode iron binding. The observed iron location, which is well determined in all of the structures, also constrains the siderophore to a position in the calyx sterically incompatible with salicylate-mode binding.

In order to confirm that the ligands are fully, or near fully, occupied, simulated-annealing composite-omit maps were calculated in CNS (Brunger et al., 1998), strictly excluding all ligand atoms. The peak heights of the electron density features corresponding to the iron atoms (Table 1) are high enough to eliminate low ligand occupancy as contributing to poor ligand density. (Siderocalin shows no appreciable affinity for iron in any form in the absence of a siderophore [Goetz et al., 2002]; therefore, any iron present in the calyx is part of a ferric siderophore complex.) What variation is seen in iron peak heights correlates well with ligand B factors, across or within individual asymmetric units, rather than reflecting lower iron occupancies in the TRECAM or TRENCAM-3,2-HOPO complexes versus the CMB complexes. Therefore, the poor quality of the ligand electron density is likely mostly a consequence of unusually pronounced ligand mobility. This conclusion is compatible with the very tight K_D in that the siderocalin recognition mechanism depends on electrostatic and cation-π interactions with few hydrogen bonds and only limited van der Waals contacts (Figure 4B). Indeed, the cationic groups are not even in van der Waals contact with any atoms of the ligands. Superposition of all the full FeEnt and DHBA/DHBS partial models of FeEnt and FeTRENCAM-3,2-HOPO from the two structures (Figure 2D) does reveal that the most constrained parts of the ligands are the catecholate moieties in pocket 1 of the trilobate calyx. This pocket, defined by the two lysine side chains (125 and 134) contributing cation-π bonds,

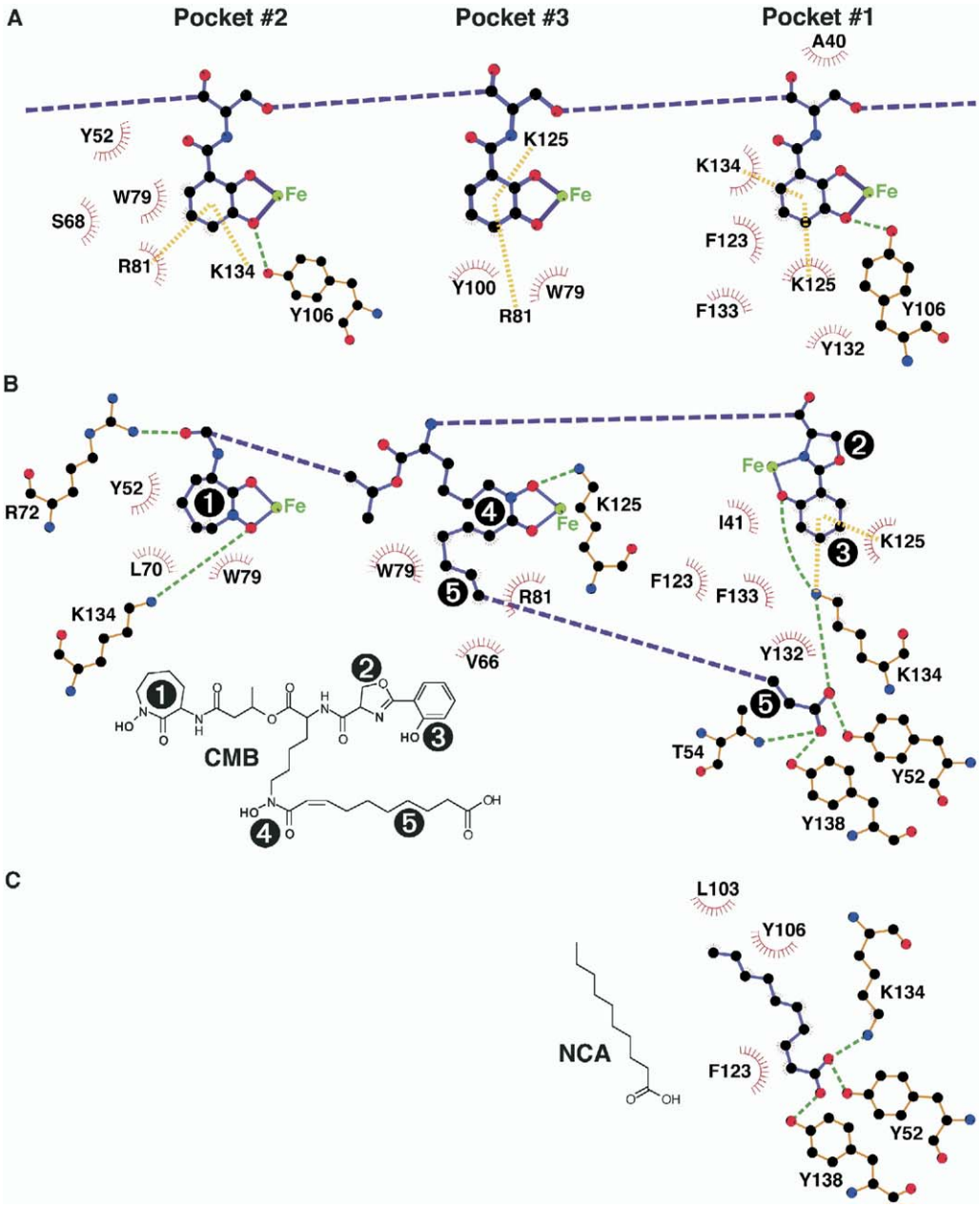

Figure 4. Exploded LIGPLOT Schematics of the Interactions between Siderocalin and Ent, CMB-S/T, and NCA, Broken Down by Calyx Pocket

(A) Ent, (B) CMB-S/T, and (C) NCA. The pictured interactions represent the union of all the protein/ligand interactions observed across all the complexes in the asymmetric unit. Ligand covalent bonds are colored purple; protein covalent bonds are colored orange. Hydrogen bonds are indicated with dashed green lines; cation-π interactions are indicated by dashed yellow bars. Atoms are colored by type (C, black; O, red; N, blue; and Fe, green). Van der Waals contacts are indicated by red sunbursts. Chemical structures for CMB (the predominant variant observed in the CMB-S crystal structures) and NCA are also shown; CMB substituent groups (1, the cyclic hydroxamate; 2, the oxazoline; 3, the phenolate; 4, the linear hydroxamate; and 5, the fatty acid tail) are numbered on the chemical structure and the corresponding parts of the LIGPLOT diagram for clarity.

is thus revealed as likely the key pocket for binding phenolate-type siderophores.

Siderocalins Bind a Variety of Phenolate and CMB Siderophores

In order to address whether siderocalin could bind ferric siderophores other than FeEnt, a panel of 18 additional, representative, natural and synthetic siderophores was qualitatively tested for binding by surface plasmon resonance (SPR), copurification and, when possible, confirmed by cocrystallization and the presence of a fully or near-fully occupied iron peak (Table 1). While the SPR assay remains a quick, simple and powerful method to qualitatively test for ligand binding, fitting the kinetic data to model binding curves remains challenging due to the complexity of the multiphasic

association and dissociation phases (data not shown). The slow component/s of the dissociation phase also prevent the system from achieving equilibrium within a reasonable time, precluding the estimation of K_D from equilibrium responses. Siderophores negative for siderocalin binding in the SPR assay also fail to bind when soaked in excess with the protein at millimolar concentrations; resultant concentrated protein solutions are unchanged in color after washing (data not shown). These results show that, as expected, siderocalin binds to a family of phenolate/catecholate siderophores chemically related to Ent but not to yeast and bacterial siderophores based on hydroxamate or α-hydroxycarboxylate iron binding groups. However, quite unexpectedly, siderocalin also binds the heterogeneous, mixed-type, soluble carboxymycobactin siderophores of *Mycobacterium smegmatis* (CMB-S) and *M. tuberculosis* (CMB-T) (Gobin et al., 1995; Lane et al., 1998, 1995; Wong et al., 1996). These compounds are quite distinct chemically from FeEnt and its relatives, with iron binding moieties contributed by 2-hydroxyphenyloxazoline, a seven-cyclic hydroxamate and a linear hydroxamate trailing off into a fatty acid tail (Figure 1). CMBs vary species to species and within a single species in the length of the fatty acid tail and by the identity of several substituent groups (Figure 1). As predicted from the pattern of sequence conservation in the calyx, murine siderocalin displays an equivalent binding specificity for the panel of 18 siderophores (data not shown).

CMBs More Completely Fill the Siderocalin Calyx, Binding in a Single Orientation

In order to elucidate the details of the interaction between siderocalin and CMB ligands, complexes between siderocalin and either FeCMB-S or -T were crystallized and analyzed crystallographically at 2.1 or 2.2 Å resolution, respectively (Table 1; Figures 2–4). The FeCMB ligands occupy a volume in the calyx overlapping that of FeEnt, with the 2-hydroxyphenyloxazoline group sitting in pocket 1, the cyclic hydroxamate group sitting in the upper part of pocket 2 and the linear hydroxamate sitting in pocket 3 (Figure 2B). The fatty acid tail curls under the rest of the siderophore, crossing from pocket 3 into pocket 1, positioning the carboxylate group into the bottom of pocket 2. Interestingly, the CMB carboxylate essentially superimposes on the carboxylate group of an adventitious ligand, tentatively identified as *n*-capric acid (NCA), in the original crystal structure of siderocalin expressed recombinantly in a baculovirus system (Goetz et al., 2000) (Figures 2C and 3C). Lysines 125 and 134 participate in cation-π bonds to the CMB hydroxybenzoyl moiety completely analogous to those in Ent, with the hydroxybenzoyl of CMB superimposing almost identically onto the DHBA moiety of Ent in pocket 1. However, largely due to the orientation of the fatty acid tail, CMBs fill the calyx more completely, generating more extensive hydrogen bond and van der Waals networks (Figure 4). The result is that the CMB ligands sit fully resolved in the calyx in a single, well-defined orientation (Figures 2E, 3B, and 4C). The most constrained portion of the CMB structure is again the hydroxybenzoyl group sitting in pocket 1. The iron atoms in the CMB complex structures have moved as much as 2.5 Å up, out of the calyx, from their positions in the Ent complexes. The linear hydroxamate and the linking elements ("backbone") of CMB make the fewest siderocalin contacts, again analogous to the Ent complex.

Binding either CMB-S or CMB-T results in essentially identical crystal structures (Figure 2E). Even though heterogeneous CMB mixtures, isolated directly from culture supernatants (Lane et al., 1995; Ratledge and Ewing, 1996), were used in cocrystallizations, the electron density is clear enough, and the resolution high enough, to show that a single molecular species predominates in the calyx in both complex structures, corresponding to an aliphatic linker in the fatty acid tail eight methylene groups long. Deletion of even one methylene group from ligand models worsens the refinement statistics. The only difference between the CMB-S and -T ligand structures is the absence of the methyl group at the R4 position on the CMB-T ligands. The structures have been refined with a double bond in the fatty acid tail (between C47 and C48 in the coordinate file) as suggested by the electron density and consistent with R_{free} values monitored during rebuilding, though this assignment is by no means certain at this resolution. The CMB-T structure clearly seen in the complex structures is also one methylene group longer in the fatty acid tail than previously reported for compounds isolated from *M. tuberculosis* cultures (Gobin et al., 1995). It has so far not been possible to purify CMB variants to the homogeneity necessary to test individual isoforms for binding.

Ligand-Sensitive Calyx Structural Elements

The only structural elements in the siderocalin calyx that display any significant conformational variation in response to the presence or absence of any of the three types of ligands (NCA, phenolate-type siderophores, or CMBs) are the side chains of two residues: Trp79 and Arg81 (Figure 2F). The side chain of Trp79 is either disordered (modeled as an alanine) or adopts one of three rotamers fairly consistently, progressively moving out of the way in response to the increasing size of the various ligands. In the CMB structures, the most calyx-filling ligands, Trp79 is oriented parallel to the calyx wall, with the distal nitrogen of the imidazole moiety pointing outward. Given the difficulty in confidently modeling arginine side chain conformations, even at this resolution, the pattern is less clear, though, again, the side chain of Arg81 adopts various rotamers. The Arg81 side chain can either intercalate between catecholate rings in the FeEnt structures, providing cation-π interactions, or move away from the ligand, substituted by the side chain of Trp79 providing alternate herringbone ring stacking interactions to the ligand. In the CMB structures, the Arg81 side chains also move to positions along the calyx wall to accommodate the larger ligands. All the other calyx residue side chain conformations are markedly well conserved among the 15 views of the siderocalin structure, including the lysines (125 and 134) donating cation-π bonds to all the different siderophore ligands. The structure of the ordered solvent shell is quite variable across all of the structures, consistent with the variable crystallization

conditions and crystal contacts, both over the surface of the protein and within the calyx. Siderophore binding displaces most of the calyx waters observed in the empty structures and there are no uniformly conserved water-mediated protein/ligand interactions.

Discussion

The Siderocalin Fold Is Imperturbable

Pair-wise superposition rmsds (on all common Cαs) across the 15 siderocalin models (Goetz et al., 2000, 2002) vary from 0.54 to 0.67 Å; these numbers improve measurably if the most N-terminal two or three residues, the most variable siderocalin structural element (Figures 3A and 3B), are excluded. These structures span two different expression systems, four different crystallization conditions (from high to low salt and neutral to low pH), six different packing environments, the presence or absence of three different ligand classes, and even the presence or absence of N-linked oligosaccharide (at Asn65). After the N terminus, the next greatest flexibility is seen in the loops rimming the calyx, where even greater variation is typically seen in other lipocalins (Flower, 1996). The secondary structure elements, and their relative arrangement, are fully conserved. This behavior is consistent with observations that extreme conditions are required to denature siderocalin and release bound siderophores (Goetz et al., 2002). However, these results directly contradict conclusions based on the solution NMR structure of siderocalin (Coles et al., 1999), where structural mobility, particularly the orientation of the α helix to the β barrel, was much more marked. We conclude that the siderocalin fold is very stable and well defined. Structural stability extends to the calyx, where the only flexibility of any significance is seen in the side chains of two residues, Trp79 and Arg81. While these two side chains do move to accommodate the presence or absence of different ligands, the degree of movement is nowhere near the level of conformational flexibility typically associated with "induced-fit" recognition mechanisms. For instance, this level of binding site plasticity is considerably less than the remodeling observed in the ligand binding site of the insect ecdysone receptor, which binds disparate ecdysteroid hormones and nonsteroidal synthetic agonists (Billas et al., 2003). However, such side chain movements observed in the siderocalin calyx could account for the multiphasic association kinetics seen in the SPR experiments, where ligand approach, possibly dominated by the electrostatic component of the interaction, is fast, and establishing the optimal calyx conformation, possibly optimizing the cation-π network, is slow.

Siderocalin Tightly Binds Phenolate/Catecholate Siderophores without Securely Constraining Their Orientation, Enabling Degeneracy

By comparing the complex structures of nonhydrolyzable phenolate/catecholate siderophores with the FeEnt complex structure, optimizing crystallization conditions to minimize crystallization time, and confirming ligand occupancy by careful analysis of iron peak heights, we have shown that the poor quality of ligand electron density features is the result of marked ligand flexibility, reflecting fundamental aspects of siderocalin-mediated recognition of phenolate/catecholate-type siderophores, and is not an artifact of previous crystallographic analyses. Siderocalin has evolved a recognition mechanism that generates tight binding while tolerating such flexibility, in the absence of interactions to the most variable element of this class of microbial siderophores, the backbone linker, thus permitting siderocalin to degenerately interact with a broad range of phenolate/catecholate siderophores. Because the siderophore phenolate moiety determines bound ligand orientation, and because the most constrained portion of the ligand sits in pocket 1, we conclude that it is the highly polarized ferric hydroxybenzoyl group that is the key determinant for siderocalin binding and that pocket 1 is the key binding pocket. Reliance on cation-π bonds to highly polarized hydroxybenzoyl iron ligands, either in context of catecholate, 2-hydroxyphenyloxazoline or, potentially, HOPO groups, complements the degenerate siderocalin recognition mechanism, broadening potential responses. These conclusions are confirmed by the analysis of siderocalin/CMB complexes, where the 2-hydroxyphenyl group superimposes on the pocket 1 catecholate groups of the phenolate/catecholate-type siderophores, even though the rest of the structures of these siderophores are essentially completely different. Variable solvent structures are unlikely to contribute to degenerate recognition in that there are few water-mediated interactions. The CMB complex structures do show that many of the complex calyx features, subpockets irrelevant for the binding of phenolate/catecholate-type enterobacterial siderophores, allow for the binding of whole different classes of siderophores, broadening, in this case, potential siderocalin-mediated antibacterial defenses to mycobacteria, which are significant human pathogens. However, antimycobacterial siderocalin responses may be limited by the high selectivity of siderocalin for a single CMB species, in terms of fatty acid tail length, in both the CMB-S and -T complex structures, even though CMB mixtures were used in the cocrystallizations. While siderocalin may be able to tolerate binding of CMB variants ± one or perhaps two methylene groups in the fatty acid moieties, though likely with significant concurrent reductions in affinity, it seems unlikely that siderocalin could accommodate the extremes of the reported CMB-S/T spectrum (Figure 1), at least while retaining the overall ligand orientation seen in the current cocrystal structures. The variation seen in CMB structures may, indeed, reflect mycobacterial responses to siderocalin-mediated defenses, evidenced by the obvious success of mycobacteria as human pathogens. The efficacy of siderocalin in thwarting mycobacterial infections in vivo remains to be tested.

Are There Other Siderophore Binding Lipocalins?

While broadly and degenerately recognizing enterobacterial phenolate/catecholate siderophores and specifically interacting with at least a limited spectrum of mycobacterial CMBs, siderocalin fails to bind to many bacterial siderophores and essentially all types of fungal siderophores (Figure 1). It is likely that evading sid-

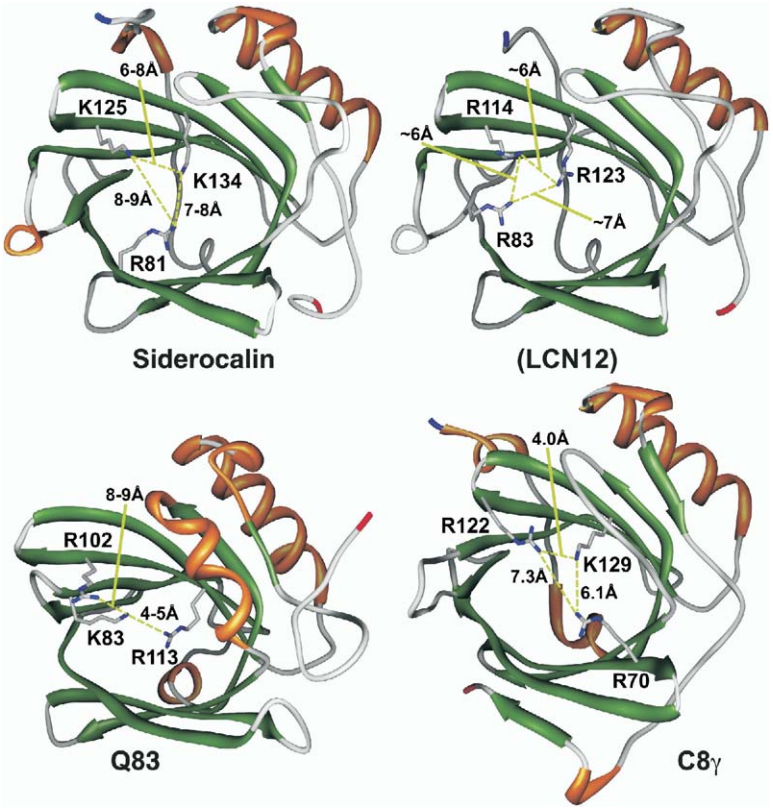

Figure 5. Ribbon Representations of Siderocalin and Three Potential Siderophore Binding Lipocalins, Colored by Secondary Structure

The side chains of characteristic triads of positively charged residues are also shown, with interresidue distances indicated. The representations are based on the crystal structures of siderocalin (1L6M.pdb) and C8γ (1IW2.pdb), the NMR structure of Q83 (1JZU.pdb), and a simplistic homology model of Lcn12 based on siderocalin using the SWISS-Model server (Peitsch, 1996). At 86% sequence identity, it is presumed that Ex-FABP will be essentially identical in structure to Q83 at this resolution. Molecular ribbons were generated with Chimera (Huang et al., 1996) (www.cgl.ucsf.edu/chimera). α, orange; β, green; and coil, gray.

erocalin contributes to virulence, as the ability to synthesize aerobactin, which does not bind to siderocalin, is a virulence factor for enteric bacteria (Wooldridge and Williams, 1993). However, it seems unusual that the innate immune system would limit such powerful anti-siderophore responses to only those pathogens whose siderophores bind to siderocalin, cleverly degenerate as it is. Since siderocalin is, to our knowledge, the first nonbacterial siderophore binding protein characterized, the search for other candidate siderophore binders must begin with neighboring lipocalins. Comparisons show that sequence identities rapidly plummet as the alignments move from the siderocalins themselves. A number of neighboring lipocalins are also readily eliminated as having characterized functions or ligands that preclude siderophore binding: the prostaglandin D_2 synthases (Helliwell et al., 2004) (~30%–35% identical to siderocalins), including distant homologs in *Xenopus* and *Bufo*, and human HC, a lipocalin associated with IgA which binds a nonsiderophore chromophore (Åkerstrom et al., 2000b) (16%–23% identical to siderocalins). However, given that the structural homology between even distantly related lipocalins is high and that the hallmark features of the siderocalin calyx (a characteristic triad of positively charged side chains) are so pronounced, it is possible to identify candidate siderophore binding lipocalins ("siderocalins").

Murine lipocalin 12 (Lcn12, 28%–29% identical to siderocalins) has recently been identified as a component of seminal fluid (Suzuki et al., 2005), but little else is known about its function. Simplistic homology modeling of Lcn12 using the SwissMODEL server (Peitsch, 1996) reveals a triad of positively charged side chains in the Lcn12 calyx completely analogous to siderocalin (Figure 5). The next most related lipocalins are the highly homologous (86% identical to each other) fowl proteins Ex-FABP (Descalzi Cancedda et al., 2000) (from chicken, ~20% identical to siderocalins) and quail Q83 (Hartl et al., 2003) (20%–22% identical to siderocalins). Ex-FABP is expressed during chicken embryo development in hypertrophic cartilage, muscle fibers, and granulocytes and is also a component of egg whites. In chondrocyte and myoblast cultures, Ex-FABP expression is induced by inflammatory agents and inhibited by anti-inflammatory agents. Q83 is a protein strongly induced in v-*myc*-transformed avian fibroblasts, though no specific candidate ligands or functions have been proposed. The NMR structure of Q83 again shows a triad of positively-charged amino acids in the calyx (conserved in Ex-FABP) very reminiscent, in arrangement and character, of the key siderophore binding residues of siderocalin (Arg81, Lys125, and Lys134), and most uncharacteristic of lipocalins in general. This arrangement is also echoed in the calyx of the more distantly related protein C8γ (Schreck et al., 2000), a well-studied member of the complement cascade and the subject of high-resolution crystallographic analyses (Ortlund et al., 2002). However, no candidate ligands for C8γ have been proposed, nor has its precise role in the membrane attack complex been delineated. However, particularly for C8γ, the shape of the calyx, at least in the absence of any hypothetical

ligand-induced conformational changes, is incompatible with the binding of any known siderocalin ligand in a comparable geometry. Nevertheless, these observations do suggest that there may be other siderophore binding lipocalins, currently unrecognized, perhaps with nonoverlapping specificities, that complement the function of siderocalin in innate immunity. Subsequent binding and crystallographic analyses, however, fail to convincingly demonstrate specific interactions between C8γ and any of the siderophores we have access to (data not shown and J.M. Sodetz, personal communication), showing that calyx elements beyond triads of positively charged residues may be necessary for siderophore binding. However, a recent report (Fluckinger et al., 2004) shows that Lcn1 (tear lipocalin, von Ebner's Gland protein), a lipocalin too distant in sequence space to have been identified in this analysis, is also functionally a "siderocalin," broadly inhibiting the growth of bacteria and fungi through ferric siderophore sequestration, though the nature of the recognition mechanism has yet to be elucidated.

Thus, proposals to use siderophores and siderophore analogs as therapeutics, either as antibiotics (Budzikiewicz, 2001; Roosenberg et al., 2000) or, through the bound iron, as oxygen radical scavengers in various clinical settings (Horwitz et al., 1998), will still need to be tempered by the possibility that endogenous siderophore binding specificities will limit, defeat, or confound such approaches.

Experimental Procedures

Protein Expression and Purification and Siderophore Binding Assays

Human siderocalin was expressed as a glutathione S-transferase fusion protein and purified as previously described (Bundgaard et al., 1994; Goetz et al., 2002). Murine siderocalin was expressed in an identical procedure. Binding of siderophores to either human or mouse siderocalin was assayed by SPR as previously described (Flo et al., 2004) using a Biacore System 3000 (Biacore AB) in HBS-P buffer. Briefly, approximately 2000–5500 resonance units (RU) of protein were coupled to research-grade CM5 sensor chips using amine coupling chemistry following the manufacturer's recommended procedure. Surface-specific activities were typically greater than 75%; siderophore responses ranged from 5 to 180 RUs. Surfaces were regenerated with 20% acetonitrile and 5 mM NaOH. A binding call corresponds to an interaction with an estimated K_D at less than 100 nM; nonbinding siderophores interact with siderocalins with a K_Ds estimated to be greater than 1 mM. Siderophores were obtained from Sigma-Aldrich, Biophore Research Products, or were synthesized (Thulasiraman et al., 1998) or isolated (Lane et al., 1995; Ratledge and Ewing, 1996) as previously described. SPR measurements of FeEnt binding are confounded by its extreme solution instability, which is not a problem for the other siderophores listed in Figure 1. All of the binding positive compounds also copurify (after extensive washing) with siderocalin, yielding obviously colored solutions, and cocrystallize with human siderocalin, though the resultant crystals are not always diffraction quality. FeEnt binding, the use of which is problematic in the SPR assay due to solution instability, has been previously demonstrated by alternate means (Goetz et al., 2002).

Crystallization and Crystallography

Siderocalin was cocrystallized with four different siderophores (TRENCAM, TRENCAM-3,2-HOPO, CMB-S, and CMB-T) using conditions that accelerated crystal growth time to 2 weeks or less from greater than 6 months (Goetz et al., 2002): vapor diffusion at 22°C over reservoirs of 1.4–1.8 M ammonium sulfate, 50–100 mM NaCl, buffered at pH 4.5 with 100 mM Na acetate. Crystals were cryopreserved in a mother liquor with 20% glycerol at –170°C. The TRENCAM complex data set was collected on a Rigaku Raxis IV area detector using CuKα radiation; the other three data sets were collected at beamlines 5.0.1 and 5.0.2 at the Advanced Light Source (Lawrence Berkeley National Laboratory, Berkeley, CA). The space group is $P4_12_12$, with three monomers in the asymmetric unit, nearly isomorphous with crystals used in the previous structure determination (Goetz et al., 2002) (Table 1). Diffraction data were processed with DENZO and SCALEPACK. Reflections reserved for calculating R_{free} (Kleywegt and Brunger, 1996) values were strictly matched between all three refined data sets. Model coordinates were refined with the CNS software package (Brunger et al., 1998) using standard protocols. Noncrystallographic symmetry restraints were not used in the refinement, consistent with R_{free} calculations. Relevant statistics are presented in Table 1. Initial model coordinates and target geometry for DHBA, used to model TRENCAM-3,2-HOPO, and CMB-S/T were derived, respectively, from the structure of enterobactin (Cambridge Structural Database entry JOSLOS) or the structures of carboxymycobactin P (Hough and Rogers, 1974) and sebacic acid (Cambridge Structural Database entry SEBAAC).

Acknowledgments

The authors wish to thank Kenneth N. Raymond (University of California, Berkeley) for much insightful input and discussion, Sudeshna Seal for assistance with crystallization, Niels Borregaard and coworkers (Rigshospitalet) for supplying MMP-9, Edward Hough for supplying ferricarboxymycobatin P (from *M. phlei*) coordinates, and James M. Sodetz and his colleagues at the University of South Carolina for providing unpublished results of their crystallographic studies of siderophore binding to C8γ. This study was supported by the National Institutes of Health (grants AI48675, AI59432, and AI11744).

Received: September 27, 2004
Revised: October 25, 2004
Accepted: October 28, 2004
Published: January 11, 2005

References

Åkerstrom, B., Flower, D.R., and Salier, J.-P. (2000a). Lipocalins: unity in diversity. Biochim. Biophys. Acta *1482*, 1–8.

Åkerstrom, B., Logdberg, L., Berggard, T., Osmark, P., and Lindqvist, A. (2000b). Alpha(1)-microglobulin: a yellow-brown lipocalin. Biochim. Biophys. Acta *1482*, 172–184.

Berman, H.M., Westbrook, J., Feng, Z., Gilliland, G., Bhat, T.N., Weissig, H., Shindyalov, I.N., and Bourne, P.E. (2000). The Protein Data Bank. Nucleic Acids Res. *28*, 235–242.

Billas, I.M., Iwema, T., Garnier, J.M., Mitschler, A., Rochel, N., and Moras, D. (2003). Structural adaptability in the ligand-binding pocket of the ecdysone hormone receptor. Nature *426*, 91–96.

Brunger, A.T., Adams, P.D., Clore, G.M., DeLano, W.L., Gros, P., Grosse-Kunstleve, R.W., Jiang, J.S., Kuszewski, J., Nilges, M., Pannu, N.S., et al. (1998). Crystallography & NMR system: a new software suite for macromolecular structure determination. Acta Crystallogr. D Biol. Crystallogr. *54*, 905–921.

Budzikiewicz, H. (2001). Siderophore-antibiotic conjugates used as trojan horses against Pseudomonas aeruginosa. Curr. Top. Med. Chem. *1*, 73–82.

Bundgaard, J.R., Sengelov, H., Borregaard, N., and Kjeldsen, L. (1994). Molecular cloning and expression of a cDNA encoding NGAL: a lipocalin expressed in human neutrophils. Biochem. Biophys. Res. Commun. *202*, 1468–1475.

Cohen, S.M., and Raymond, K.N. (2000). Catecholate/salicylate heteropodands: demonstration of a catecholate to salicylate coordination change. Inorg. Chem. *39*, 3624–3631.

Coles, M., Diercks, T., Muehlenweg, B., Bartsch, S., Zolzer, V., Tschesche, H., and Kessler, H. (1999). The solution structure and dynamics of human neutrophil gelatinase-associated lipocalin. J. Mol. Biol. *289*, 139–157.

Descalzi Cancedda, F., Dozin, B., Zerega, B., Cermelli, S., and Cancedda, R. (2000). Ex-FABP: a fatty acid binding lipocalin developmentally regulated in chicken endochondral bone formation and myogenesis. Biochim. Biophys. Acta *1482*, 127–135.

Devireddy, L.R., Teodoro, J.G., Richard, F.A., and Green, M.R. (2001). Induction of apoptosis by a secreted lipocalin that is transcriptionally regulated by IL-3 deprivation. Science *293*, 829–834.

Dougherty, D.A. (1996). Cation-π interactions in chemistry and biology: a new view of benzene, Phe, Tyr, and Trp. Science *271*, 163–168.

Ecker, D.J., Matzanke, B.F., and Raymond, K.N. (1986). Recognition and transport of ferric enterobactin in Escherichia coli. J. Bacteriol. *167*, 666–673.

Ecker, D.J., Loomis, L.D., Cass, M.E., and Raymond, K.N. (1988). Substituted complexes of enterobactin and synthetic analogs as probes of the ferric-enterobactin receptor in *Escherichia coli*. J. Am. Chem. Soc. *110*, 2457–2464.

Flo, T.H., Smith, K.D., Sato, S., Rodriguez, D.J., Holmes, M.A., Strong, R.K., Akira, S., and Aderem, A. (2004). Lipocalin 2 mediates a novel innate immune response to bacterial infection by sequestrating iron. Nature *432*, 917–921.

Flower, D.R. (1996). The lipocalin protein family: structure and function. Biochem. J. *318*, 1–14.

Flower, D.R., North, A.C., and Sansom, C.E. (2000). The lipocalin protein family: structural and sequence overview. Biochim. Biophys. Acta *1482*, 9–24.

Fluckinger, M., Haas, H., Merschak, P., Glasgow, B.J., and Redl, B. (2004). Human tear lipocalin exhibits antimicrobial activity by scavenging microbial siderophores. Antimicrob. Agents Chemother. *48*, 3367–3372.

Gobin, J., Moore, C.H., Reeve, J.R., Jr., Wong, D.K., Gibson, B.W., and Horwitz, M.A. (1995). Iron acquisition by Mycobacterium tuberculosis: isolation and characterization of a family of iron-binding exochelins. Proc. Natl. Acad. Sci. USA *92*, 5189–5193.

Goetz, D.H., Willie, S.T., Armen, R.S., Bratt, T., Borregaard, N., and Strong, R.K. (2000). Ligand preference inferred from the structure of neutrophil gelatinase associated lipocalin. Biochemistry *39*, 1935–1941.

Goetz, D.H., Holmes, M.A., Borregaard, N., Bluhm, M.E., Raymond, K.N., and Strong, R.K. (2002). The neutrophil Lipocalin NGAL is a bacteriostatic agent that interferes with siderophore-mediated iron acquisition. Mol. Cell *10*, 1033–1043.

Guex, N., and Peitsch, M.C. (1997). SWISS-MODEL and the Swiss-PdbViewer: an environment for comparative protein modeling. Electrophoresis *18*, 2714–2723.

Hartl, M., Matt, T., Schuler, W., Siemeister, G., Kontaxis, G., Kloiber, K., Konrat, R., and Bister, K. (2003). Cell transformation by the v-myc oncogene abrogates c-Myc/Max-mediated suppression of a C/EBP β-dependent lipocalin gene. J. Mol. Biol. *333*, 33–46.

Helliwell, R.J., Adams, L.F., and Mitchell, M.D. (2004). Prostaglandin synthases: recent developments and a novel hypothesis. Prostaglandins Leukot. Essent. Fatty Acids *70*, 101–113.

Horwitz, L.D., Sherman, N.A., Kong, Y., Pike, A.W., Gobin, J., Fennessey, P.V., and Horwitz, M.A. (1998). Lipophilic siderophores of Mycobacterium tuberculosis prevent cardiac reperfusion injury. Proc. Natl. Acad. Sci. USA *95*, 5263–5268.

Hough, E., and Rogers, D. (1974). The crystal structure of ferrimycobactin P, a growth factor for the mycobacteria. Biochem. Biophys. Res. Commun. *57*, 73–77.

Huang, C.C., Couch, G.S., Pettersen, E.F., and Ferrin, T.E. (1996). Chimera: an extensible molecular modeling application constructed using standard components. Pacific Symposium on Biocomputing *1*, 724.

Kamezaki, K., Shimoda, K., Numata, A., Aoki, K., Kato, K., Takase, K., Nakajima, H., Ihara, K., Haro, T., Ishikawa, F., et al. (2003). The lipocalin 24p3, which is an essential molecule in IL-3 withdrawal-induced apoptosis, is not involved in the G-CSF withdrawal-induced apoptosis. Eur. J. Haematol. *71*, 412–417.

Kjeldsen, L., Cowland, J.B., and Borregaard, N. (2000). Human neutrophil gelatinase-associated lipocalin and homologous proteins in rat and mouse. Biochim. Biophys. Acta *1482*, 272–283.

Kleywegt, G.J., and Brunger, A.T. (1996). Checking your imagination: applications of the free R value. Structure *4*, 897–904.

Lane, S.J., Marshall, P.S., Upton, R.J., Ratledge, C., and Ewing, M. (1995). Novel extracellular mycobactins, the carboxymycobactins from Mycobacterium avium. Tetrahedron Lett. *36*, 4129–4132.

Lane, S.J., Marshall, P.S., Upton, R.J., and Ratledge, C. (1998). Isolation and characterization of carboxymycobactins as the second extracellular siderophores in *Mycobacterium smegmatis*. Biometals *11*, 13–20.

Laskowski, R.A., MacArthur, M.W., Hutchinson, E.G., and Thornton, J.M. (1992). PROCHECK: a program to check the stereochemical quality of protein structures. J. Appl. Crystallogr. *26*, 283–291.

Matzanke, B.F., Ecker, D.J., Yang, T.S., Huynh, B.H., Muller, G., and Raymond, K.N. (1986). Escherichia coli iron enterobactin uptake monitored by Mossbauer spectroscopy. J. Bacteriol. *167*, 674–680.

Nizet, V., Ohtake, T., Lauth, X., Trowbridge, J., Rudisill, J., Dorschner, R.A., Pestonjamasp, V., Piraino, J., Huttner, K., and Gallo, R.L. (2001). Innate antimicrobial peptide protects the skin from invasive bacterial infection. Nature *414*, 454–457.

Ortlund, E., Parker, C.L., Schreck, S.F., Ginell, S., Minor, W., Sodetz, J.M., and Lebioda, L. (2002). Crystal structure of human complement protein C8γ at 1.2 A resolution reveals a lipocalin fold and a distinct ligand binding site. Biochemistry *41*, 7030–7037.

Peitsch, M.C. (1996). ProMod and Swiss-Model: internet-based tools for automated comparative protein modelling. Biochem. Soc. Trans. *24*, 274–279.

Ratledge, C., and Ewing, M. (1996). The occurrence of carboxymycobactin, the siderophore of pathogenic mycobacteria, as a second extracellular siderophore in Mycobacterium smegmatis. Microbiol. *142*, 2207–2212.

Raymond, K.N., Müller, G., and Matzanke, B.F. (1984). Complexation of iron by siderophores. A review of their solution and structural chemistry and biological function. In Topics in Current Chemistry, F.L. Boschke, ed. (Berlin: Springer-Verlag), pp. 50–102.

Raymond, K.N., Dertz, E.A., and Kim, S.S. (2003). Enterobactin: an archetype for microbial iron transport. Proc. Natl. Acad. Sci. USA *100*, 3584–3588.

Roosenberg, J.M., 2nd, Lin, Y.M., Lu, Y., and Miller, M.J. (2000). Studies and syntheses of siderophores, microbial iron chelators, and analogs as potential drug delivery agents. Curr. Med. Chem. *7*, 159–197.

Salzman, N.H., Ghosh, D., Huttner, K.M., Paterson, Y., and Bevins, C.L. (2003). Protection against enteric salmonellosis in transgenic mice expressing a human intestinal defensin. Nature *422*, 522–526.

Schreck, S.F., Parker, C., Plumb, M.E., and Sodetz, J.M. (2000). Human complement protein C8γ. Biochim. Biophys. Acta *1482*, 199–208.

Stintzi, A., and Raymond, K.N. (2002). Siderophore chemistry. In Molecular and Cellular Iron Transport, D.M. Templeton, ed. (Toronto: Marcel Dekker, Inc.), pp. 273–320.

Suzuki, K., Lareyre, J.-J., Sánchez, D., Gutierrez, G., Araki, Y., Matusik, R.J., and Orgebin-Crist, M.C. Molecular evolution of a multigene subfamily encoding epididymal lipocalins localized on the [A3] locus of mouse chromosome 2. Gene, in press.

Thulasiraman, P., Newton, S.M., Xu, J., Raymond, K.N., Mai, C., Hall, A., Montague, M.A., and Klebba, P.E. (1998). Selectivity of ferric enterobactin binding and cooperativity of transport in gram-negative bacteria. J. Bacteriol. *180*, 6689–6696.

Tschesche, H., Zolzer, V., Triebel, S., and Bartsch, S. (2001). The human neutrophil lipocalin supports the allosteric activation of matrix metalloproteinases. Eur. J. Biochem. *268*, 1918–1928.

Wallace, A.C., Laskowski, R.A., and Thornton, J.M. (1995). LIG-

PLOT: a program to generate schematic diagrams of protein-ligand interactions. Protein Eng. *8*, 127–134.

Wilson, C.L., Ouellette, A.J., Satchell, D.P., Ayabe, T., Lopez-Boado, Y.S., Stratman, J.L., Hultgren, S.J., Matrisian, L.M., and Parks, W.C. (1999). Regulation of intestinal α-defensin activation by the metalloproteinase matrilysin in innate host defense. Science *286*, 113–117.

Winkelmann, G. (2002). Microbial siderophore-mediated transport. Biochem. Soc. Trans. *30*, 691–696.

Wong, D.K., Gobin, J., Horwitz, M.A., and Gibson, B.W. (1996). Characterization of exochelins of Mycobacterium avium: evidence for saturated and unsaturated and for acid and ester forms. J. Bacteriol. *178*, 6394–6398.

Wooldridge, K.G., and Williams, P.H. (1993). Iron uptake mechanisms of pathogenic bacteria. FEMS Microbiol. Rev. *12*, 325–348.

Xu, S., and Venge, P. (2000). Lipocalins as biochemical markers of disease. Biochim. Biophys. Acta *1482*, 298–307.

Yang, J., Goetz, D., Li, J.Y., Wang, W., Mori, K., Setlik, D., Du, T., Erdjument-Bromage, H., Tempst, P., Strong, R., et al. (2002). An iron delivery pathway mediated by a lipocalin. Mol. Cell *10*, 1045–1056.

Accession Numbers

Atomic coordinates for the complexes of siderocalin with CMB-S, CMB-T, and the partial model of TRENCAM-3,2-HOPO have been deposited in the Protein Data Bank (Berman et al., 2000) with accession numbers 1X89, 1X8U, and 1X71, respectively.